PERGAMON

Chemical Engineering Science 56 (2001) 2085–2102

Chemical Engineering Science

www.elsevier.nl/locate/ces

Dynamic behaviour of reactive distillation columns described by a nonequilibrium stage model

R. Baur[a], R. Taylor[b], R. Krishna[a,*]

[a]Department of Chemical Engineering, University of Amsterdam, Nieuwe Achtergracht 166, 1018 WV Amsterdam, The Netherlands
[b]Department of Chemical Engineering, Clarkson University, Potsdam, NY 13699-5705, USA

Received 27 December 1999; accepted 20 October 2000

Abstract

In this paper we develop a generic, dynamic, nonequilibrium (NEQ) stage model for reactive distillation (RD) columns. The main features of our model are: (1) use of the Maxwell–Stefan equations for describing mass transfer between fluid phases, (2) solid catalysed reactions are treated using a pseudo-homogeneous liquid phase model with the appropriate pseudo-homogeneous kinetic expressions and (3) a comprehensive set of design correlations, for both trays (sieve, bubble caps) and packings (random dumped, structured), for hold-up and mass transfer have been incorporated into the software package following earlier work (Taylor et al., *Comput. Chem. Eng.* 18 (1994) 205). We report some interesting dynamic features of RD columns by examining the response of a column for methyl *tert*-butyl ether (MTBE) synthesis to perturbations in the feed of methanol, iso-butene or n-butene. When operating at a high-conversion branch of the bifurcation diagram, small perturbations are shown to lead to a transition to a low-conversion branch. The NEQ model is shown to be more susceptible to feed perturbations than a conventional equilibrium (EQ) model with constant component efficiencies. The differences between the dynamic behaviour of trayed and random-packed columns are also emphasised in this work. The dynamic behaviour of the column has been interpreted on the basis of the iso-butene recycle flow in the column. It has been shown that the size, type and duration of a feed perturbation causing a transition from one to another steady state depends on the model description, on the column configuration and on the residence time distribution along the column height. Experimental verification of the developed dynamic model is obtained by comparison with the experimental results of Mohl et al. (*Chem. Eng. Sci.* 54 (1999) 1029) for synthesis of tertiary amyl ether (TAME).

Keywords: Reactive distillation; Equilibrium stage model; Nonequilibrium stage model; Multiple steady states; Nonlinear dynamics; Maxwell–Stefan equations; Methyl tert-butyl ether synthesis

1. Introduction

In their influential review article on reactive distillation (RD), Doherty and Buzad (1992) wrote "... steady state simulations are inadequate for assessing the effectiveness of operability and control schemes for reactive distillation columns... control schemes with good steady state measures frequently fail under dynamic conditions, and that the failure was discovered only by using the full nonlinear dynamic simulation. ....There are good opportunities for productive research in this area, including such effects as the existence of multiple steady states in reactive distillation and strategies for operating at the desired one". This statement is supported by anecdotal evidence in the literature on the complex behaviour of RD pilot plant columns (Bravo, Pyhalathi, & Jaervelin, 1993).

To describe the dynamics of RD columns, three types of models exist in the literature (a comprehensive review is available in Taylor and Krishna (2000):

(1) equilibrium (EQ) stage model (Abufares & Douglas, 1995; Bartlett & Wahnschafft, 1998; Espinosa, Martinez, & Perez, 1994; Grosser, Doherty, & Malone, 1987; Kumar & Daoutidis, 1999; Moe, Hauan, Lien, & Hertzberg, 1995; Perez-Cisneros, Schenk, Gani, & Pilavachi, 1996; Scenna, Ruiz, & Benz, 1998; Schrans, de Wolf, & Baur, 1996; Sneesby, Tadé, & Smith, 1998b);
(2) EQ stage model with fixed stage efficiencies (Alejski & Duprat, 1996; Ruiz, Basualdo, & Scenna, 1995) and

* Corresponding author. Tel.: +31-20-525-7007; fax: +31-20-525-5604.
E-mail address: krishna@its.chem.uva.nl (R. Krishna).

0009-2509/01/$ - see front matter
PII: S0009-2509(00)00496-6

(3) nonequilibrium (NEQ) stage model for packed RD column (Kreul, Gorak, Dittrich, & Barton, 1998).

The primary objective of the current paper is to first develop a rigorous dynamic NEQ model for RD columns, for both sieve tray and randomly packed configurations. The model development presented here is an extension of the steady-state NEQ model for RD columns published earlier (Baur, Higler, Taylor, & Krishna, 2000; Higler, Taylor, & Krishna, 1998, 1999c,d; Higler, Krishna, & Taylor, 1999a,b, 2000). With the developed NEQ model we study the differences in the RD column dynamics predicted by the NEQ model with the more widely used EQ model (often with a stage efficiency). We study the differences in the dynamics of two typical RD hardware configurations, a sieve tray column and a randomly packed column. Experimental verification of the developed dynamic model is obtained by comparison with the experimental results of Mohl et al. (1999) for synthesis of tertiary amyl ether (TAME).

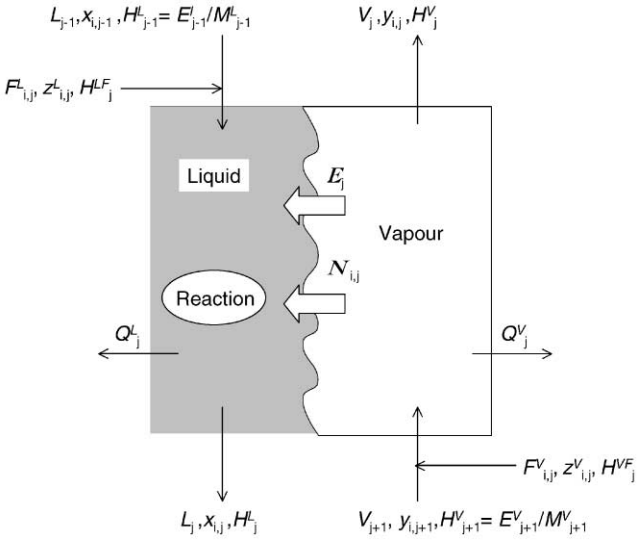

Fig. 1. Schematic representation of an NEQ stage.

2. Dynamic nonequilibrium (NEQ) model development

2.1. Balance relations

The dynamics of a stage are determined, inter alia, by the storage capacity, or accumulation, of mass and energy in the vapour and liquid phase on any given stage. We develop below the transient balances for a contacting stage portrayed in Fig. 1. Both the vapour and liquid phases on the stage are assumed to be well mixed. The time rate of change of the number of moles of component i in the vapour (M_i^V) and liquid (M_i^L) phases on stage j are given by the following balance relations:

$$\frac{\mathrm{d}M_{i,j}^V}{\mathrm{d}t} = V_{j+1}y_{i,j+1} - V_j y_{i,j} + z_{i,j}^V F_{i,j}^V - \mathbb{N}_{i,j}^V, \quad i = 1,2,\ldots,c, \tag{1}$$

$$\frac{\mathrm{d}M_{i,j}^L}{\mathrm{d}t} = L_{j-1}x_{i,j-1} - L_j x_{i,j} + z_{i,j}^L F_{i,j}^L + \mathbb{N}_{i,j}^L + \sum_{k=1}^{r} \nu_{i,k} R_{k,j} \varepsilon_j^L, \quad i = 1,2,\ldots,c, \tag{2}$$

where $\mathbb{N}_{i,j}$ is the interfacial mass transfer rate. A total of r chemical reactions take place in the liquid phase and $R_{k,j}$ is the rate of reaction k on stage j, $\nu_{i,k}$ represents the stoichiometric coefficient of component i in reaction k and ε_j^L represents the volumetric liquid hold-up on stage j. Heterogeneous chemical reactions taking place inside catalyst particles are taken account of by using a pseudo-homogeneous description by use of catalyst effectiveness factors and effective reaction rate constants (Higler et al., 2000; Sundmacher & Hoffmann, 1994). The feed entering the column at any inlet is treated as follows. The liquid portion of this feed enters the feed tray specified and the vapour portion enters the tray above. The feed flow rate of component i in the vapour phase to stage j is $z_{i,j}^V F_{i,j}^V$ and the feed flow rate of component i in the liquid phase to stage j is $z_{i,j}^L F_{i,j}^L$ where $z_{i,j}^V$ and $z_{i,j}^L$ are the corresponding mole fractions of the feed streams. In order to determine these quantities the program includes adiabatic and fixed T–p flash calculation routines.

The overall molar balances are obtained by summing Eqs. (1) and (2) over the total number of components, c in the mixture:

$$\frac{\mathrm{d}M_j^V}{\mathrm{d}t} = V_{j+1} - V_j + F_j^V - \sum_{k=1}^{c} \mathbb{N}_{k,j}^V, \tag{3}$$

$$\frac{\mathrm{d}M_j^L}{\mathrm{d}t} = L_{j-1} - L_j + F_j^L + \sum_{k=1}^{c} \mathbb{N}_{i,j}^L + \sum_{i=1}^{c}\sum_{k=1}^{r} \nu_{i,k} R_{k,j} \varepsilon_j^L. \tag{4}$$

The mole fractions of the vapour and liquid phases are calculated from the respective phase molar hold-ups:

$$y_{i,j} = \frac{M_{i,j}^V}{M_j^V}, \qquad x_{i,j} = \frac{M_{i,j}^L}{M_j^L}, \quad i = 1,2,\ldots,c-1. \tag{5}$$

Only $c-1$ of these mole fractions are independent because the phase mole fractions sum to unity:

$$\sum_{k=1}^{c} y_{k,j} = 1, \qquad \sum_{k=1}^{c} x_{k,j} = 1. \tag{6}$$

In our model $c-1$ molar component balances (1) and (2) have been implemented along with Eqs. (3)–(6).

The energy balances for the vapour and liquid phases are written in terms of the energy "hold-ups" in the vapour and liquid phases on stage j:

$$\frac{dE_j^V}{dt} = V_{j+1}\frac{E_{j+1}^V}{M_{j+1}^V} - V_j\frac{E_j^V}{M_j^V} + F_j^V H_j^{VF} - \mathbb{E}_j^V - Q_j^V, \quad (7)$$

$$\frac{dE_j^L}{dt} = L_{j-1}\frac{E_{j-1}^L}{M_{j-1}^L} - L_j\frac{E_j^L}{M_j^L} + F_j^L H_j^{LF} + \mathbb{E}_j^L - Q_j^L, \quad (8)$$

where $\mathbb{E}_j$ represents the interphase energy transfer rate and Q_j the heat addition (or removal) via external heat exchange. The energy hold-ups are related to the corresponding molar hold-ups via the stage enthalpies

$$E_j^V = H_j^V M_j^V, \qquad E_j^L = H_j^L M_j^L. \quad (9)$$

There is no need to take separate account in Eq. (8) of the heat generated due to chemical reaction since the computed enthalpies include the heats of formation. The phase temperatures T_j^V and liquid T_j^L are determined from the corresponding phase enthalpies using an ideal or excess enthalpy model.

2.2. Interfacial mass and energy transfers

The resistance to mass and energy transfer is assumed to be located in thin "films" adjacent to the vapour–liquid interface; see Fig. 2. The liquid phase diffusion film thickness δ^{Lf} is of the order of 10 μm and the vapour phase diffusion film thickness δ^{Vf} is of the order of 100 μm. The storage capacity for mass and energy in these films is negligibly small compared to that in the bulk fluid phases and so the interfacial transfer rates can be calculated from quasi-stationary interfacial transfer relations. For transfer within the vapour phase diffusion film (superscript Vf) we have

$$\frac{\partial \mathbb{N}_i^{Vf}(\eta^{Vf})}{\partial \eta^{Vf}} = 0, \quad (10)$$

$$\frac{\partial \mathbb{E}^{Vf}}{\partial \eta^{Vf}} = 0. \quad (11)$$

Here η^{Vf} represents the dimensionless distance along the liquid diffusion path: $\eta^{Vf} = 0$ at the edge of the film (of thickness δ^{Vf}) and $\eta^{Vf} = 1$ at the vapour–liquid interface; see Fig. 2. The interfacial transfer rates are constant across the vapour phase diffusion film. The situation within the liquid phase diffusion film is more complex for we need to take account of the chemical reaction within this film:

$$\frac{\partial \mathbb{N}_i^{Lf}(\eta^{Lf})}{\partial \eta^{Lf}} + \sum_{k=1}^{r} \nu_{i,k} R_k(\eta^{Lf}) A\delta^{Lf} = 0, \quad (12)$$

$$\frac{\partial \mathbb{E}^{Lf}}{\partial \eta^{Lf}} = 0. \quad (13)$$

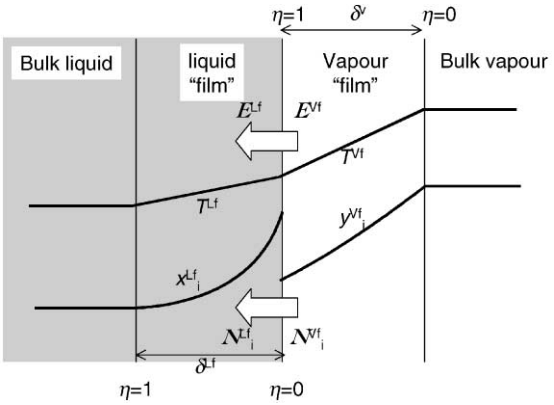

Fig. 2. Composition and temperature profiles within the vapour and liquid "films". The NEQ model takes account of the enhancement of the mass transfer due to chemical reaction within the diffusion film in the liquid close to the interface.

A represents the interfacial area and $A\delta^{Lf}$ represents the volume available for liquid phase chemical reaction. The coupling of diffusion and chemical reaction within the liquid film is particularly important for fast chemical reactions (Hatta number exceeding unity). For solid catalysed chemical reactions our approach is to use pseudo-homogeneous reaction rates; in such cases there will be no coupling of chemical reaction and diffusion within the liquid film.

In order to solve Eqs. (10)–(13) for each stage j in the column we need constitutive relations for the interfacial mass and energy transfer rates. The molar transfer rate $\mathbb{N}_i^{Lf}$ in the liquid phase is related to the chemical potential gradients by the Maxwell–Stefan equations (Krishna & Wesselingh, 1997; Taylor & Krishna, 1993; Wesselingh & Krishna, 2000)

$$\frac{x_i^{LF}}{\mathbb{R}T^{Lf}}\frac{\partial \mu_i^{Lf}}{\partial \eta} = \sum_{k=1}^{c} \frac{x_i^{LF}\mathbb{N}_k^{Lf} - x_k^{LF}\mathbb{N}_i^{Lf}}{c_t^{Lf}\kappa_{i,k}^{Lf} A}, \quad i = 1,2,\ldots,c. \quad (14)$$

$\kappa_{i,k}^{Lf}$ represents the mass transfer coefficient of the i–k pair in the liquid phase; this coefficient is estimated from information on the corresponding Maxwell–Stefan diffusivity $Đ_{i,k}^L$ using the standard procedures discussed in Taylor and Krishna (1993). Only $c-1$ of Eq. (14) are independent. The summation equations hold:

$$\sum_{k=1}^{c} y_{i,j}^{VF} = 1, \qquad \sum_{k=1}^{c} x_{i,j}^{LF} = 1. \quad (15)$$

The interphase energy transfer rates $\mathbb{E}^{Lf}$ have conductive and convective contributions

$$\mathbb{E}^{Lf} = -h^{Lf} A\frac{\partial T^{Lf}}{\partial \eta} + \sum_{i=1}^{c} \mathbb{N}_i^{Lf} H_i^{Lf}, \quad (16)$$

where h^{Lf} is the heat transfer coefficient in the liquid phase. A relation analogous to Eq. (16) holds for the vapour phase.

At the vapour–liquid interface we assume phase equilibrium

$$y_i|_I - K_i x_i|_I = 0, \qquad T^{Vf}|_I = T^{Lf}|_I, \tag{17}$$

where the subscript I denotes the equilibrium compositions and K_i is the vapour–liquid equilibrium ratio for component i. At the interface we have continuity of mass and energy:

$$\mathbb{N}_i^{Vf}|_I = \mathbb{N}_i^{Lf}|_I, \qquad \mathbb{E}^{Vf}|_I = \mathbb{E}^{Lf}|_I. \tag{18}$$

2.3. Properties, hydrodynamics and mass transfer

The NEQ model requires thermodynamic properties, not only for calculation of phase equilibrium but also for calculation of driving forces for mass transfer and, in reactive distillation, for taking into account the effect of nonideal component behaviour in the calculation of reaction rates and chemical equilibrium constants. In addition, physical properties such as surface tension, diffusion coefficients, viscosities, etc. for calculation of mass (and heat) transfer coefficients and interfacial areas are required. For the most part the property models we use are those recommended by Reid, Prausnitz, and Poling (1988) and by Danner and Daubert (1983). The details of the models used for estimation of diffusivities are discussed in standard texts (Reid et al., 1988; Seader & Henley, 1998; Taylor & Krishna, 1993).

In the dynamic NEQ model, hardware design information must be specified so that mass transfer coefficients, interfacial areas, liquid hold-ups and pressure drops can be calculated. A listing of the correlations for tray and packed columns implemented in the program is given in Baur et al. (2000) and Taylor, Kooijman, and Hung (1994). The theory behind the tray and packed column design is available in Fair, Steinmeyer, Penney, and Croker (1997), Kooijman (1995), Lockett (1986), Stichlmair and Fair (1998) and Taylor and Krishna (1993). Interested readers can download the technical manual from the ChemSep website: http://www.clarkson.edu/~chengweb/faculty/taylor/chemsep/chemsep.html, which contains details of all thermodynamics, hydrodynamics and mass transfer models for tray and packed columns which have already been implemented into our reactive distillation software. The code for these models represents a large fraction of the overall program size.

For a sieve tray column, for example, the volumetric liquid hold-up on the tray can be calculated from knowledge of the active (or bubbling) tray area, A_{bub}, and estimation of the clear liquid height, h_{cl}:

$$\frac{1}{c_{t,j}^L} M_j^L \equiv \varepsilon_j^L = h_{\mathrm{cl},j} A_{\mathrm{bub},j}. \tag{19}$$

The clear liquid height can be estimated from correlations of Bennett, Agrawal, and Cook (1983) or Barker and Self (1962). If the tray spacing is h_t, the volumetric hold-up of the vapour phase can be calculated from

$$\frac{1}{c_{t,j}^V} M_j^V \equiv \varepsilon_j^V = (h_t - h_{\mathrm{cl},j}) A_{\mathrm{bub},j}. \tag{20}$$

2.4. Summary of model equations for a single stage

Table 1 summarises the set of equations describing the vapour and liquid phases for a single stage. The number of differential equations on a single stage is $2c + 2$. The partial differential equations that describe mass transfer through the vapour and liquid films are discretised over the film thickness by application of a finite difference scheme, with fixed grid points.

2.5. Condenser and reboiler configuration

The liquid hold-up in the reboiler and condenser is usually much larger than the hold-up on a particular stage. High liquid hold-ups lead to operational robustness, but also cause the equations to be very stiff. In our dynamic NEQ model implementation, liquid buffers are incorporated at the top and bottom, as indicated in Fig. 3. The partial, or total, condenser is followed by a reflux drum buffering the condensate. A partial condenser is modelled as an equilibrium stage (Seader & Henley, 1998). The reflux drum is considered to be a well-mixed system with a specified volumetric capacity. The mean liquid residence time and dynamic characteristics are therefore fully determined with this specification. There is an option to consider liquid phase reactions taking place in the reflux drum and in the reboiler; in the simulations presented below we did not consider such reactions.

The liquid leaving the bottom of the column is led to a reboiler drum with a specified volumetric capacity (hold-up) and assumed to be well mixed. The contents are then transferred to a partial, or total reboiler. A partial reboiler is modelled as an equilibrium stage.

2.6. Numerical solution

The resulting set of differential-algebraic (DAE) equations is solved using BESIRK (Kooijman, 1995; Kooijman & Taylor, 1995). BESIRK is a semi-implicit Runge–Kutta method originally developed by Michelsen (1976) and extended with an extrapolation scheme (Bulirsch & Stoer, 1966), improving the efficiency in solving the DAE problem. The evaluation of the sparse Jacobian is primarily based on analytical expressions, except for the computation of entries for correlations like enthalpies, mass and heat transfer coefficients, hold-ups and pressure drops.

Our program also supports steady-state computations using Newton's method, as outlined in Taylor et al. (1994). In addition, the program is equipped with a

Table 1
Model equations for single-stage nonequilibrium model. The model equations are either ordinary differential equations (ODE), partial differential equations (PDE), or algebraic equations (AE). The number of discrete points in the liquid film is denoted with nL, and in the vapour film with nV

		Bulk liquid phase			Bulk vapour phase		
Description of equation	Number of equations	Type	Eq. no.	Var.	Number of equations	Eq. no.	Var.
Total molar balance	1	ODE	Eq. (4)	M_i^L	1	Eq. (3)	M_i^V
Molar component balance	$c-1$	ODE	Eq. (2)	$M_{i,j}^L$	$c-1$	Eq. (1)	$M_{i,j}^V$
Mole fractions	c	AE	Eq. (5)	$x_{i,j}$	c	Eq. (5)	$y_{i,j}$
Summation	1	AE	Eq. (6)		1	Eq. (6)	
Energy balance	1	ODE	Eq. (8)	E^L	1	Eq. (7)	E^V
Energy hold-up	1	AE	Eq. (9)	T_j^L	1	Eq. (9)	T_j^V
Volumetric hold-up	1	AE	Eq. (19)	L	1	Eq. (20)	V
		"Film" liquid phase			"Film" vapour phase		
Molar component balance	$nL\times c$	PDE	Eq. (12)	$\mathbb{N}_{i,j}^{Lf}$	c	Eq. (10)	$\mathbb{N}_{i,j}^{Lf}$
Maxwell–Stefan equations	$nL\times(c-1)$	PDE	Eq. (14)	x_{ij}^{Lf}	$nV\times(c-1)$	Eq. (14)	y_{ij}^{Vf}
Summation	$nL\times 1$	AE	Eq. (15)		$nV\times 1$	Eq. (15)	
Energy balance	$nL\times 1$	PDE	Eq. (13)	$\mathbb{E}_j^{Lf}$	$nV\times 1$	Eq. (11)	$\mathbb{E}_j^{Lf}$
Energy transfer rate	$nL\times 1$	PDE	Eq. (16)	T_j^{Lf}	$nV\times 1$	Eq. (16)	T_j^{Vf}
Total: $(5c+8+nL\times(2c+2)+nV\times(c+2))$ implemented equations per stage							

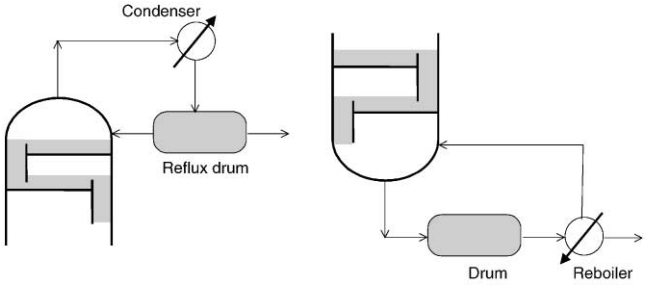

Fig. 3. Condenser and reboiler model configurations.

continuation method for analysis of multiple steady-state behaviour. For more details about this continuation method the reader is referred to Wayburn and Seader (1987) and Kubicek (1976).

The simulations have been performed on a PC (Pentium II 286 MHz). An NEQ model with 17 stages contains approximately 2000 equations and requires about 30 min computing time to reach a new steady state following a perturbation. An EQ stage model has about 300 equations, and needs only a couple of minutes for the same problem.

3. Dynamics of sieve tray RD column: EQ vs. NEQ models

In order to illustrate the dynamics of RD columns we undertook a case study involving the synthesis of methyl *tert*-butyl ether (MTBE). The column configuration chosen for the simulations is shown in Fig. 4; this is the configuration described by Jacobs and Krishna (1993) in their simulation study using the EQ stage model. The total number of stages is 17, including a total condenser and a partial reboiler; the column pressure is 1115 kPa. Reactive stages are located in the middle of the column, stage 4 down to and including stage 11. The column has two feed streams: a methanol feed and a mixed butenes feed. A small stoichiometric excess of methanol is used. The mixed butenes feed, to stage 11, contains a mixture of iso-butene, which is reactive, and n-butene, which is nonreactive or inert. The reflux ratio is set to 7 and the reboiler heat duty is either set to 39.87 MW or varied (as a continuation parameter). The product removed from the top of the column is predominantly the inert n-butene. The bottoms product consists predominantly of MTBE. For a properly designed and operated column it is possible to achieve close to 100% conversion of iso-butene.

The column diameter was chosen to be 6 m. The stripping, rectifying and reactive sections consist of sieve trays. The configurations of the sieve trays are: total tray area = 28.27 m^2; number of liquid flow passes = 5; tray spacing = 0.7 m; liquid flow path length = 0.97 m; fractional active area = 0.76; fractional hole area = 0.1; fractional downcomer area = 0.12; hole diameter = 4.5 mm; weir height = 50 mm; total weir length = 22 m; weir type = segmental; downcomer clearance = 0.0381 m; tray deck thickness = 25 mm. The five-liquid-pass tray

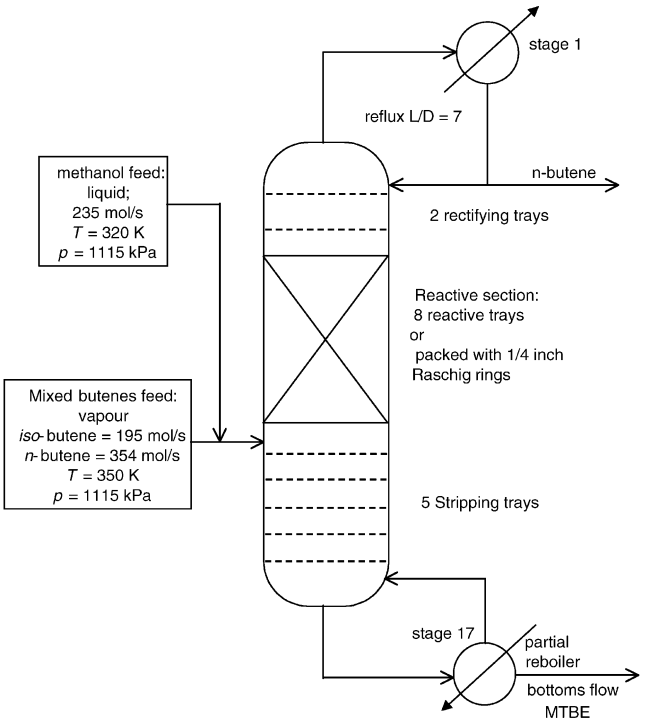

Fig. 4. Configuration of the MTBE synthesis column, following Jacobs and Krishna (1993). The column consists of 17 stages. The reactive stages are configured either as sieve trays (see Fig. 5) or packed with catalytically active Raschig rings.

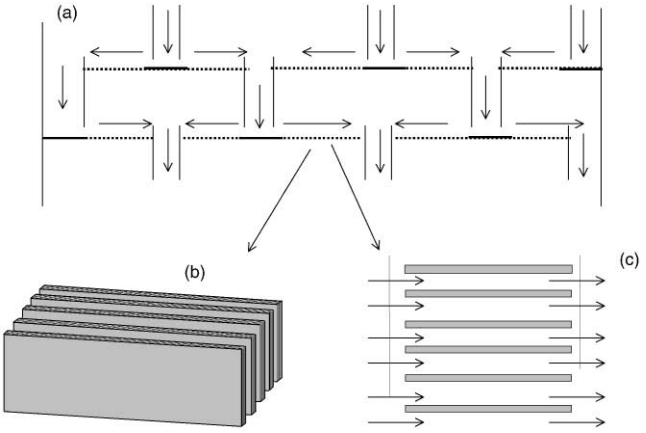

Fig. 5. (a) Five-liquid-pass sieve tray configuration. (b) and (c) The reactive section consists of catalyst envelopes placed along the liquid flow path.

configuration is shown in Fig. 5(a). On each of the eight stages in the reactive zone, 1000 kg of catalyst is introduced in the form of "envelopes" placed along the flow path length; see Fig. 5(b) and (c). The details of such a construction are available in the patent literature (Jones, 1985). The total amount of catalyst in the reactive zone is 8000 kg. The ion-exchange capacity of the catalyst is 4.54 meq H^+/g. The capacity of the reflux drum is taken to be 1.3 m^3 and that of the reboiler drum is 2.3 m^3.

The UNIQUAC model was used for description of liquid phase nonideality, while the Soave–Redlich–Kwong equation of state was used for the vapour phase. The extended Antoine equation was used for calculation of the vapour pressure. Thermodynamic and kinetic data are taken from Rehfinger and Hoffmann (1990a,b).

The first objective of our dynamic RD simulations is to compare the results of EQ and NEQ models. The separation capability of the nonreactive stripping and rectifying sections will also affect the overall column performance. We decided to focus on the differences of the EQ and NEQ modelling of the reactive section only and, therefore, assumed the nonreactive stages to have equal separation capability in both implementations. Towards this end, in the EQ model implementation we have assumed a tray efficiency of 65% for the nonreactive rectifying stages and 58% for the nonreactive stripping stages; these values corresponded closely to the calculations of the NEQ model for the corresponding nonreactive rectifying and stripping sections using the *A.I.Ch.E.* calculation method for sieve tray mass transfer (for details of this model see Lockett, 1986) and the Hofhuis and Zuiderweg (1979) correlation for the estimation of the interfacial area. For both EQ and NEQ models, the fractional liquid hold-up on the tray is estimated from the correlation of Barker and Self (1962). Of course, in the NEQ model implementation of the nonreactive stages, efficiencies are not used in the calculations but can be calculated from the simulation results; these stage efficiencies vary for individual components.

Güttinger and Morari (1999a,b) have shown using an EQ stage model that the phenomenon of multiple steady states in RD is related to the specification of the bottom *molar* flow rate as bifurcation parameter. They have shown that use of the mass flow rate makes the multiplicity disappear. We first tried to confirm their conclusions employing the NEQ model. When using the molar bottoms flow steady-state multiplicity is indeed observed with the NEQ model; see Fig. 6(a). Also, in conformity with the results of Güttinger and Morari (1999a,b), when the bottoms flow rate is expressed in volumetric terms, this multiplicity disappears; see Fig. 6(b).

We carried out a series of steady-state simulations, using the reboiler heat duty as continuation parameter; see Fig. 6(c) and (d). For various component efficiencies in the reactive section the bifurcation diagrams were obtained as shown in Fig. 6(d). The best match with the rigorous steady-state NEQ model was obtained when the component efficiencies in the reactive section were all taken to be 0.8; see Fig. 6(c). In the dynamic simulations to be reported below, we take $E = 0.8$ in the reactive section. Furthermore, the reboiler heat duty is taken as 39.87 MW. At this reboiler load three steady states are obtained: (a) a high-conversion state, (b) a low-conversion state and (c) an intermediate, unstable state.

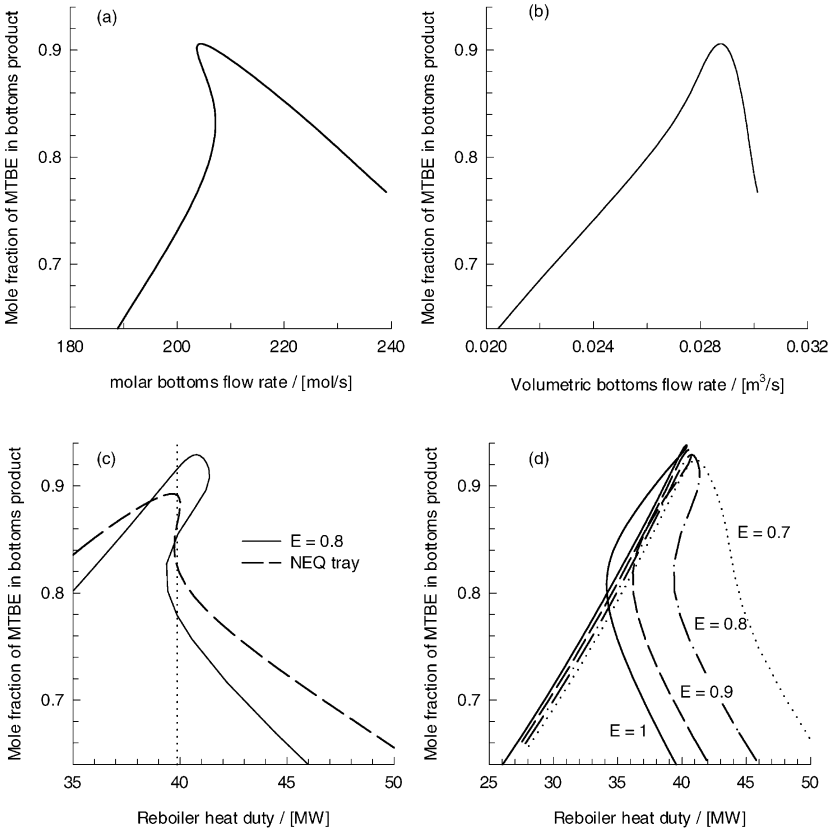

Fig. 6. Bifurcation diagram for NEQ model using (a) molar and (b) volumetric bottoms flow rate as continuation parameter. (c) Comparison of the bifurcation diagram for NEQ model with EQ model taking $E = 0.8$ for reactive section. (d) Bifurcation diagram for sieve tray configuration for various efficiency values in the reactive section.

We performed dynamic simulations of the RD columns, starting with the high-conversion steady-state situation, and introducing a perturbation in the feed, 1 h after start-up and lasting 1 h. Fig. 7 shows the MTBE mole fraction in the bottom product stream predicted by EQ and NEQ models for, respectively, methanol, isobutene and n-butene feed flow rate perturbations.

For the EQ model, the system reverts back to the initial steady state after the methanol feed was decreased by 7% during the 1 h disturbance; see Fig. 7(a). Increasing the perturbation duration up to 4 h, however, causes a steady-state transition from the high-conversion branch to the low-conversion branch of the bifurcation diagram shown in Fig. 6(c). The dynamic response of the NEQ model is quantitatively different. The system suffers already a steady-state transition when the methanol feed is perturbed for 1 h. Fig. 7(b) and (c) shows a similar system behaviour for EQ and NEQ models. For a 1 h perturbation with 7% increase of the iso-butene feed the EQ model predicts the system to revert back to its initial high-conversion steady state, whereas the NEQ model does not. As shown in Fig. 7(c), the same observation holds for a 1 h perturbation with 7% decrease of the n-butene feed. When the size of the perturbation is increased to -10%, however, both EQ and NEQ models suffer steady-state transitions from high- to low-conversion states; see Fig. 7(d).

Starting at the low-conversion branch in Fig. 6(c), Fig. 8(a) shows the dynamic response of the column to a $+15\%$ methanol feed perturbation. The EQ model recovers to its initial (low) conversion steady state. On the other hand, the NEQ model enjoys a transition to the high-conversion state. For a $+7\%$ perturbation in the n-butene feed, both EQ and NEQ models undergo transitions from low- to high-conversion states; see Fig. 8(b). Fig. 8(c) shows the dynamic response of the column to a -5% iso-butene feed perturbation. The EQ model recovers to its initial (low) conversion steady state. On the other hand, the NEQ model ascends to the high-conversion state. For a -7% perturbation in the iso-butene feed, both EQ and NEQ models migrate from low- to high-conversion states; see Fig. 8(d).

As can be seen from the examples above, transitions from one steady state to another can be triggered depending on type, size and duration of a perturbation. In order to understand the foregoing phenomena we have to focus on the MTBE production within the reactive section. A column operating at a high-conversion

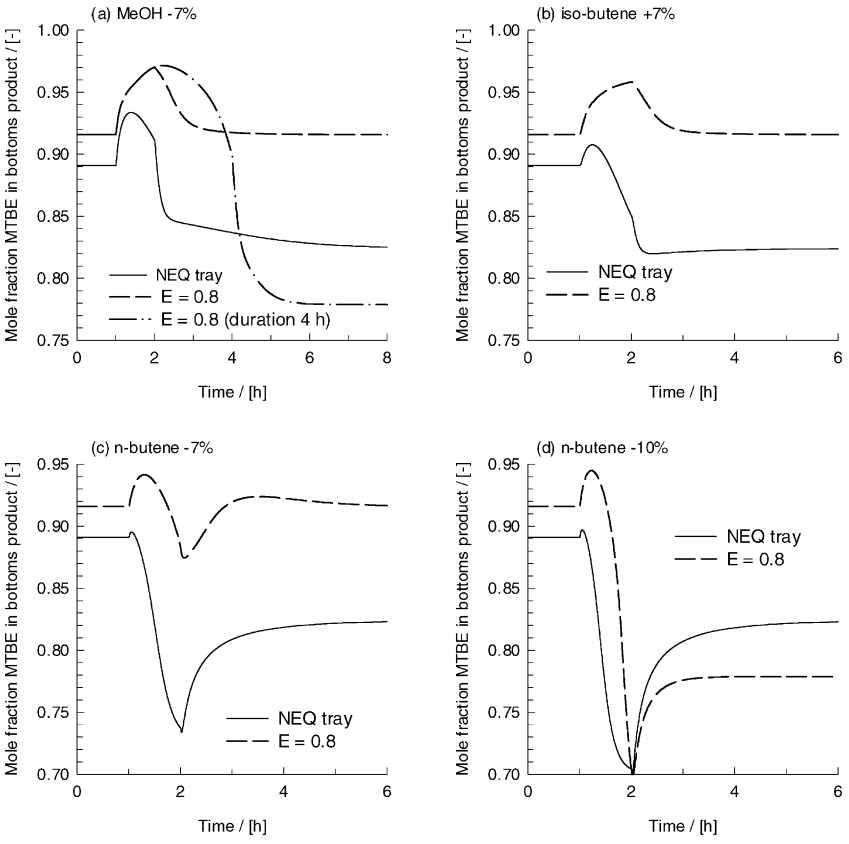

Fig. 7. Dynamic responses of bottoms product temperature to (a) − 7% MeOH, (b) + 7% iso-butene, (c) − 7% n-butene and (d) − 10% n-butene, 1 h after column start-up. Starting steady state is the high-conversion one. Comparison of EQ and NEQ models for tray column configuration.

steady state typically exhibits increasing MTBE production rates from the top to the bottom of the reactive section, where hardly any MTBE is decomposed (Hauan, Hertzberg, & Lien, 1995; Baur et al., 2000). When operating at a low-conversion steady state, a significant amount of MTBE is already produced in the top section of the reactive zone, close to the rectifying section. Consequently, MTBE accumulates towards the bottom of the reactive zone until chemical equilibrium is reached and the reaction starts to proceed in the reverse direction. On these stages a significant amount of MTBE is decomposed into methanol and iso-butene, resulting in a lower overall iso-butene conversion. Therefore, the low-conversion steady state typically exhibits a larger internal iso-butene recycle flow through the condenser with higher iso-butene concentration in the rectifying section.

Sneesby, Tadé, and Smith (1998a) have remarked that the accompanying temperature rise suppresses the synthesis reaction due to its exothermic nature. This was also observed for the MTBE process studied in this paper. When eliminating the temperature dependence of the reaction by maintaining the reaction kinetics constant, the region of multiplicity shrinks significantly but does not vanish. This indicates that reaction kinetics are not the sole cause of multiple steady states; there are additional factors such as the vapour–liquid equilibrium and interactions between reactive and nonreactive column sections (Güttinger & Morari, 1999).

Since the column is fed with a small stoichiometric excess of methanol, a transition from one steady state to another steady state depends predominantly on the size of the iso-butene recycle flow and, thus on the flows and on the iso-butene concentration in the rectifying section. Operating at a low-conversion steady state, a decrease of the iso-butene concentration in the rectifying section could possibly result in an extinction of the MTBE production at the top of the reactive section causing a shift from a low- to a high-conversion steady state. On the contrary, an increase of iso-butene in the rectifying section possibly triggers a transition from a high- to a low-conversion steady state.

In order to illustrate this let us consider the steady-state transition shown in Fig. 7(a). The NEQ model predicts a transition from a high- to a low-conversion steady state when the methanol feed is decreased by 7% for 1 h. Fig. 9 presents the column profiles of the internal liquid molar flow and the mole fractions of the reactants iso-butene and methanol at three points in time: the start

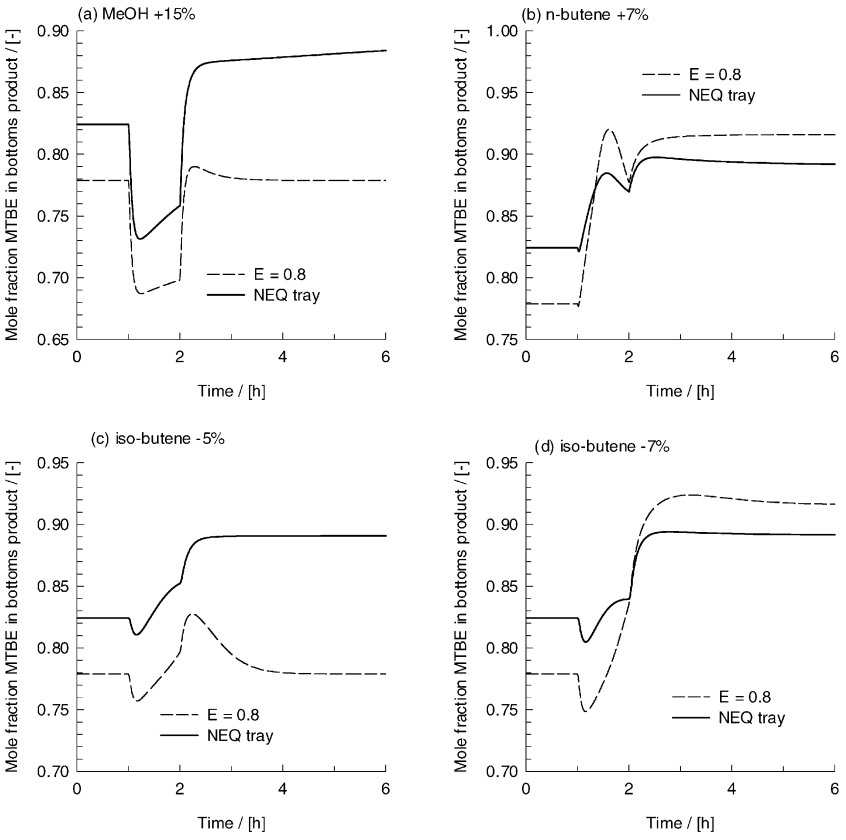

Fig. 8. Dynamic response to (a) + 15% MeOH, (b) + 7% n-butene, (c) − 5% iso-butene and (d) − 7% iso-butene feed flow perturbations, 1 h after column start-up and lasting for 1 h. Starting steady state is the low-conversion one. Comparison of EQ and NEQ models for tray column configuration.

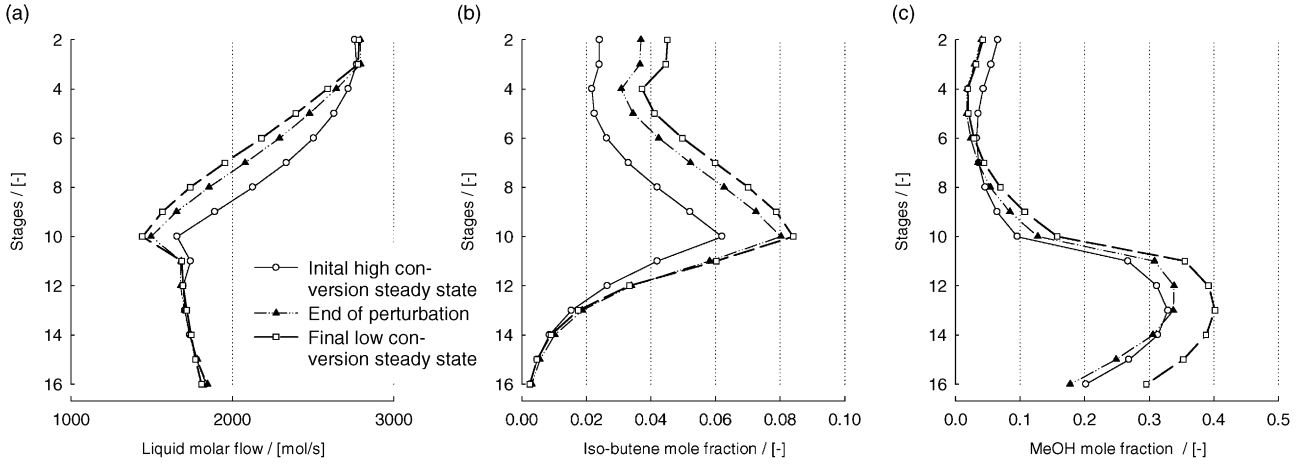

Fig. 9. Column profiles predicted by the NEQ model for the liquid molar flow rate, iso-butene and MeOH mole fraction at $t = 1$,2 and 25 h. The MeOH feed flow is perturbed by − 7%. 1 h after column start-up. The initial steady state is the high-conversion one.

of the perturbance ($t = 1$ h), its end ($t = 2$ h) and when the column reached the final low-conversion steady state ($t = 25$ h).

The internal flows in the stripping section depend on the reboiled liquid, hence on the heat of vaporisation of the reboiler mixture and the specified reboiler load. For the configurations studied, the reboiler contains mainly pure MTBE and its heat duty is fixed. This results in nearly constant internal flows along the stripping section over time; see Fig. 9(a). A feed perturbation, in turn, will mainly affect the internal flows along the reactive section. In case of a decreased methanol feed, less methanol is

converted to MTBE in the beginning of the perturbation. The unconsumed iso-butene, however, rises towards the rectifying section. This leads to an increased MTBE production in the upper part of the reactive zone and, on the other hand, causes later on an MTBE accumulation and decomposition in the reactive stages close to the stripping section. The gradual increase of methanol on stages 9–13 indicates the rising MTBE decomposition during the disturbance; see Fig. 9(c). Already at the end of the perturbation, $t = 2$ h, the iso-butene concentrations in the rectifying section are significantly higher; see Fig. 9(b). When the methanol feed is reset to its original value, the reaction rates at the top of the reactive zone and the MTBE decomposition at the bottom do not allow the system to revert back to its initial (high-conversion) steady state. Obviously, this underlying mechanism is not triggered for a 7% methanol feed increase. In that case additional iso-butene is already consumed at the beginning of the perturbation and a sufficient large iso-butene recycle will never be reached.

Analogous considerations hold for other perturbations. For example, an increase of the iso-butene or a decrease of the inert feed flow will enrich the rectifying section with iso-butene, since both components have roughly the same volatility. Therefore, transitions from a high- to low-conversion steady state are possible, as presented in Fig. 8(c) and (d), but not from a low- to high-conversion steady state.

The column performance can be strongly influenced by mass transfer when operating at a low-conversion steady state (Baur et al., 2000). Increased mass transfer resistance tends to a narrow the region of multiplicity. This is due to the fact that the iso-butene mass transfer rates are very close to the iso-butene consumption rates when operating in a low-conversion steady state. Increasing the mass transfer resistance mitigates the MTBE production in the top and the MTBE decomposition in the bottom of the reactive section. The overall iso-butene conversion will become higher and, therefore, the iso-butene recycle flow through the condenser lower.

For the cases studied above, we previously observed that an increase or decrease of the iso-butene recycle flow determines whether a system reverts to its initial steady state or undergoes a transition to another steady state. In Figs. 8 and 9 we compared the dynamic response with those of an EQ model using a Murphree efficiency of 0.8 in the reactive zone. The average component efficiency recomputed from the results of the NEQ model for both high- and low-conversion steady state is approximately 0.7. A corresponding EQ model does not reveal a region of multiplicity when employing an efficiency of 0.7; see Fig. 6(d). The employed Murphee efficiency in the EQ model is greater than the averaged component efficiencies of the NEQ model. This indicates that the EQ model predicts higher separation and so less mass transfer resistance in the reactive section than the NEQ model does. Accordingly, the iso-butene recycle and the reaction rates predicted by the NEQ model are smaller, too. This makes the NEQ model more susceptible to perturbations than an EQ model. One should keep in mind that both models employ the same hydrodynamic correlations and exhibit a similar residence time distribution along the column height. This is why the considerations above can be based on the steady-state performance of the NEQ and EQ models. In the next paragraph we will see that differences in the residence time distribution along the column height also have a significant impact on the column dynamics.

The observations described in the previous section are also reflected in a two-parameter bifurcation diagram. Fig. 10(a) shows the bifurcation diagram for NEQ model

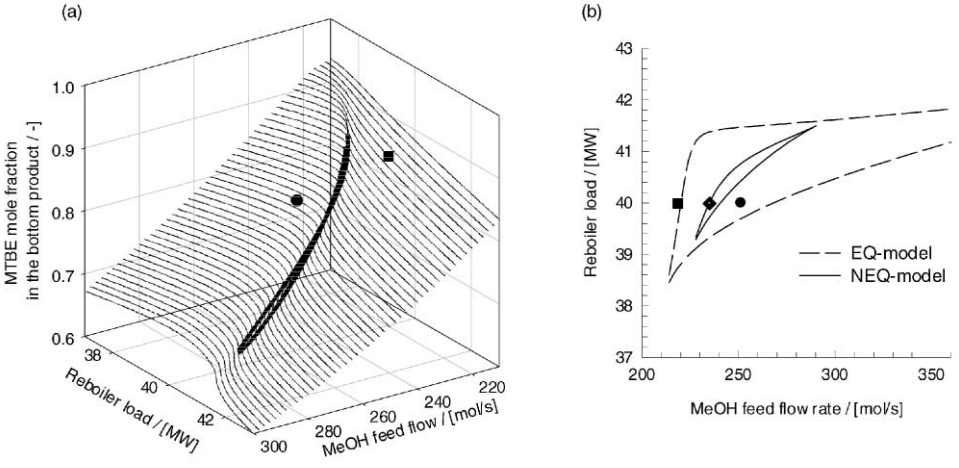

Fig. 10. (a) Bifurcation diagram for the NEQ model in dependence of reboiler load and MeOH feed flow. The solid lines indicate the turning points of the fold bifurcation. (b) Region of multiplicity displayed in the parameter space of the MeOH feed flow and reboiler load. The solid line shows the region of multiplicity predicted by the NEQ model and the dashed line predicted by the EQ model with 0.8 efficiency.

as a function of reboiler load and methanol feed flow. The latter parameter is subsequently used as the perturbation parameter. The solid lines indicate the turning points of the fold bifurcation. Projecting these turning points on the two-parameter space, we can identify a region of multiplicity; see solid line in Fig. 10(b). The dashed line in Fig. 10(b) shows the turning points of the bifurcation diagram for the EQ model. Note that the effect of enhanced separation in the reactive section results in a significantly larger region where multiplicity can be found.

We consider now the NEQ model in some more detail (similar considerations are also applicable to the EQ model). The diamond marker in Fig. 10(b) denotes the base case configuration with a reboiler load of 39.87 MW and a methanol feed flow of 235 mol/s, as it has been used for the perturbations in Figs. 7 and 8. The circle and square show the location of perturbed steady states when the methanol feed is varied by $\pm 7\%$. Both perturbed steady states are lying outside the region of multiplicity. Keeping the reboiler load constant at 39.87 MW, we see from Fig. 10(a) that the perturbed steady state with increased methanol feed flow belongs to the high-conversion branch. The perturbed steady state exhibits similar temperature, composition and reaction profiles as the high-conversion steady state at the base case specification. On the contrary, the perturbed steady state with a decreased methanol feed flow belongs to a low-conversion steady-state branch.

As observed in Fig. 7(a) a decrease of the methanol feed flow can cause a transition from the high- to low-conversion steady state, but no transition was observed from a low- to a high-conversion steady state. This is clear when considering that the perturbed steady state belongs to the low-conversion branch. On the other hand, the system possibly enjoys a transition from the low- to the high-conversion steady state when methanol feed is increased; see Fig. 8(a). In this case the perturbed steady state is lying on the high-conversion branch.

Generally speaking, if the initial and the perturbed steady states located outside a region of multiplicity are lying on the same branch and exhibit similar column profiles a transition from one steady state to another is not possible. On the other hand, if they are located on different branches a transition is very well possible.

Let us now consider the situation where we use the molar bottom flow rate as continuation parameter. Fig. 11(a) shows the bifurcation diagram for NEQ model as a function of the molar bottom flow rate and methanol feed flow; the latter is used as the perturbation parameter. The region of multiplicity is displayed in Fig. 11(b). We have chosen a molar bottom flow rate of 210 mol/s and a methanol feed of 235 mol/s as base case configuration; see diamond in Fig. 11(b). The perturbed steady states with $+7$ and -7% methanol feed flow rates are not located in the region of multiplicity; see square and circle markers in Fig. 11(b). In contrast to the reboiler load specification, shown in Fig. 10, the perturbed steady state with an increased methanol feed is located on the low-conversion branch, whereas the perturbed steady state with a decreased methanol feed is located on the high-conversion branch. From this observation we would expect that a transition from high- to low-conversion steady state is only possible if the methanol feed were increased during the perturbation. As can be seen from Fig. 12 this is true. A 1 h perturbation with 7% increase of the methanol feed causes a transition from a high- to a low-conversion steady state. For a -7% methanol feed flow perturbation the system reverts back to the initial (high) steady state.

The dynamic response observed in Fig. 12 requires further physical explanation. Fig. 13 shows the column profiles of the liquid flow and the mole fractions of the

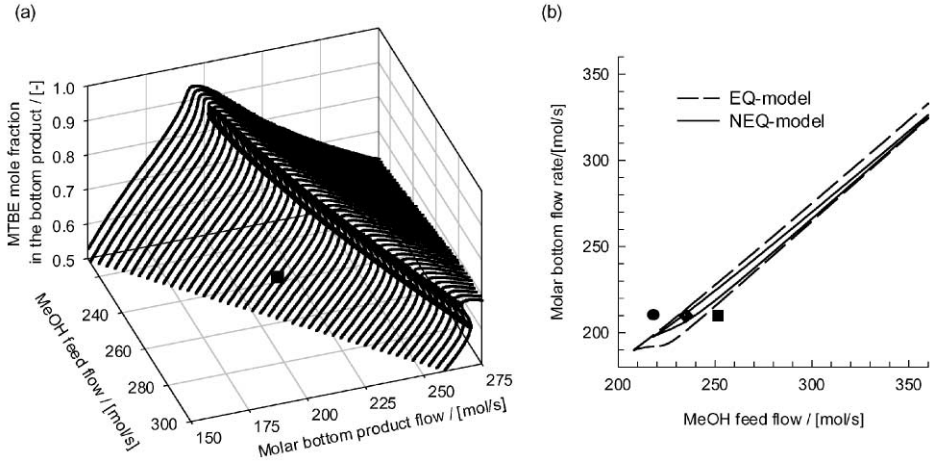

Fig. 11. (a) Bifurcation diagram for the NEQ model as a function of molar bottom flow rate and MeOH feed flow. The solid lines indicate the turning points of the fold bifurcation. (b) Region of multiplicity displayed in the parameter space of the MeOH feed flow and molar bottom flow rate. The solid eline shows the region of multiplicity predicted by the NEQ model and the dashed line predicted by the EQ model with 0.8 efficiency.

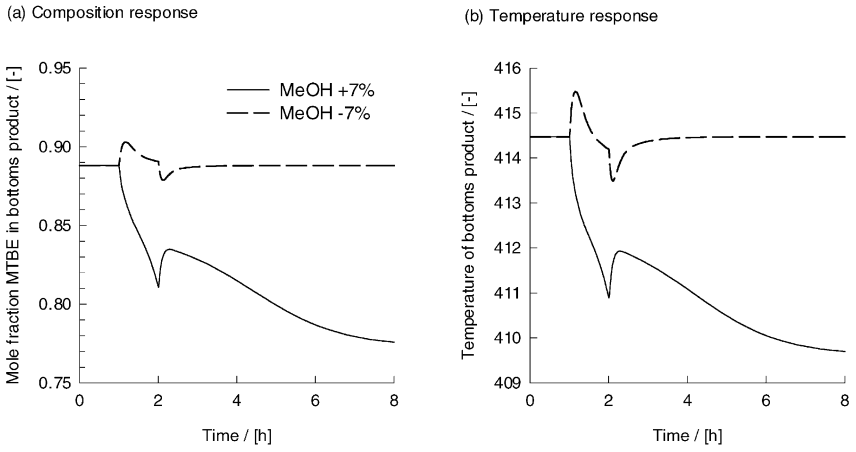

Fig. 12. Dynamic response of the NEQ model to + 7 and − 7% feed flow perturbations, 1 h after column start-up and lasting for 1 h. Starting steady state is the high-conversion one. The reboiler configuration was specified with a constant molar bottoms flow rate of 210 mol/s.

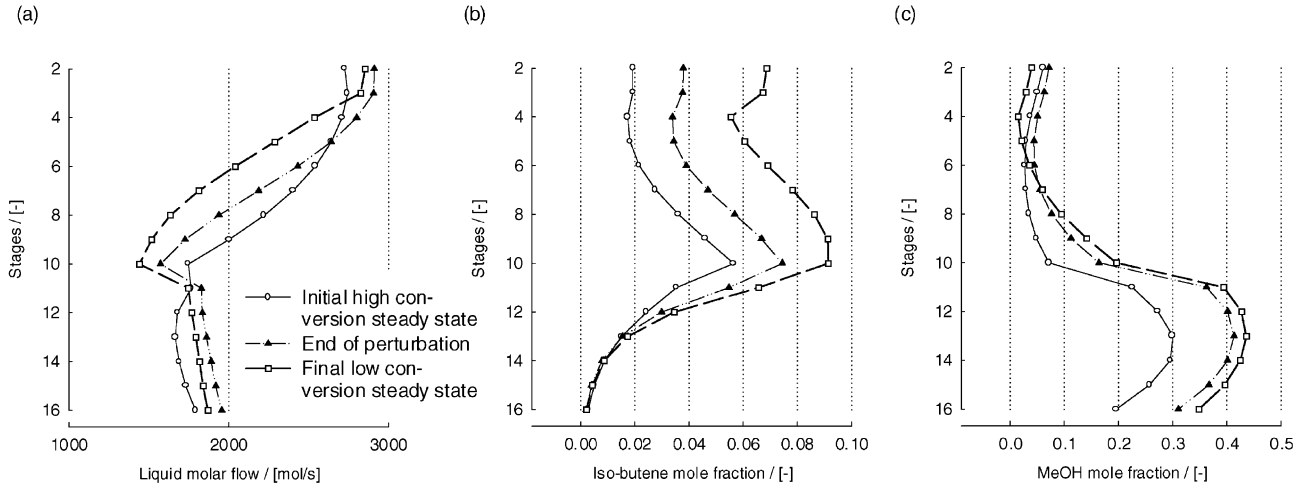

Fig. 13. Column profiles predicted by the NEQ model for the liquid molar flow rate, iso-butene and MeOH mole fraction at $t = 1$,2 and 25 h. The MeOH feed flow is perturbed by + 7% 1 h after column start-up. The initial steady state is the high-conversion one. The reboiler configuration was specified with a constant molar bottom flow rate of 210 mol/s.

reactants for a + 7% methanol feed flow perturbation when the molar bottom flow rate is taken to be 210 mol/s. Since the molar bottom flow rate is kept constant, an increase or a decrease of the feed flow rate directly affects the internal molar flow rates along the entire column. Consequently, the enlarged methanol flow pushes iso-butene towards the rectifying section; see Fig. 13. Already at the end of the perturbation, $t = 2$ h, a large amount of methanol is distributed within the column and iso-butene has been accumulated in the reactive and rectifying section. This causes a higher MTBE production in the top of the reactive section and MTBE decomposition in the bottom, respectively. After 1 h the feed is reset, but the system does not return to its initial (high) conversion steady state any more.

The example above shows that the column specifications have a significant impact on the open loop dynamics. Although, multiple steady states have been observed for both column specifications, fixed reboiler heat duty and fixed molar bottom flow rate, these two column specifications do not always respond in the same manner with respect to feed flow perturbations. Table 2 summarises the predicted steady-state transitions depending on perturbations in the feed flow. It is worth noting that the response of MeOH feed perturbation is opposite for fixed reboiler duty and fixed molar bottom flow rate.

4. Dynamics of sieve tray vs. packed RD configurations

We now study the influence of hardware configuration on RD column dynamics. The sieve tray configuration, shown in Fig. 5(b) is compared with a column in which

Table 2
Influence of feed perturbation (up to 15%) causing a transition from one steady state to another when the reboiler heat duty or molar bottom flow rate is fixed. The table is based on the NEQ model. For fixed reboiler heat duty, qualitatively similar results are obtained with the EQ model taking constant efficiency $E = 0.8$

	Steady-state transition from high to low		Steady-state transition from low to high	
Perturbed feed flow (increase or decrease)	Fixed reboiler heat duty	Fixed molar bottoms flow rate	Fixed reboiler heat duty	Fixed molar bottoms flow rate
MeOH	Decrease	Increase	Increase	Decrease
iso-Butene	Increase	Increase	Decrease	Decrease
n-Butene	Decrease	Decrease	Increase	Increase

the reactive section is filled with catalytically active packing material in the form of 0.25 in Raschig ring-shaped ion-exchange (Amberlyst 15) catalyst packing as described by Sundmacher and Hoffmann (1994). The specifications of the reactive section are: column diameter = 6 m, reactive packed zone height = 0.7 m, specific packing surface = 600 m^2/m^3, void fraction in the column = 0.72, packing density = 410 kg/m^3, catalyst pore voidage = 0.45, ion-exchange capacity of catalyst = 4.54 meq H^+/g. The nonreactive rectifying and stripping sections are configured as sieve trays with exactly the same configuration as in the foregoing simulations. In the NEQ model for the reactive section the mass transfer coefficients are calculated using the Onda, Takeuchi, and Okumoto (1968) correlation. The 0.7 m high packed reactive section needs to be divided into a sufficient number of "slices" (= stages) for accurate calculations. Our study shows that at least 88 slices are required for acceptable accuracy. Increasing the number of slices beyond 88 does not alter the results.

The bifurcation diagrams corresponding to Fig. 6 for the sieve and packed column configurations are shown in Fig. 14. For a reboiler heat duty of 39.87 MW both configurations show steady-state multiplicity. The dynamic simulations reported below have been carried out with a reboiler duty of 39.87 MW with an initial steady state that is chosen to be either at the high- or low-conversion branches of the bifurcation diagrams.

Fig. 15(a) shows the RD column response to a -5% perturbation in the MeOH feed flow. While the tray column recovers to its initial steady state, the packed column suffers transition to the low-conversion state. Similar behaviour is observed for $+2\%$ iso-butene and -1% n-butene feed flow perturbations; see Fig. 15(b) and (c). When starting at the high-conversion state, the packed column is more sensitive to feed flow perturbations.

Fig. 16(a) shows the RD column response to a $+15\%$ increase in the MeOH feed flow when starting at the low-conversion steady state. We now note that the packed column returns to its initial state but the tray column undergoes a transition to the high-conversion

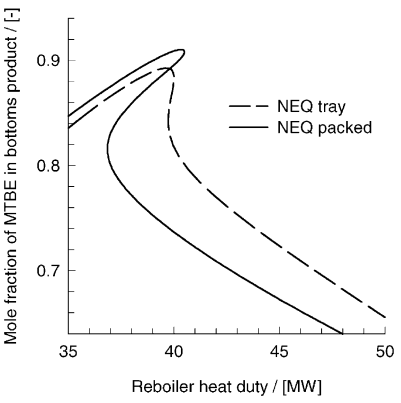

Fig. 14. Bifurcation diagrams for sieve tray and packed column configurations for MTBE synthesis. Calculations using NEQ model for both configurations.

steady state. Similar behaviour is observed for -7% iso-butene and $+3\%$ n-butene feed flow perturbations; see Fig. 16(b) and (c). When starting at the low-conversion state, the tray column is more sensitive to feed flow perturbations than the packed column.

In order to understand this behaviour we have to extend our previous explanations. The packed column configuration is a hybrid column containing dumped packing in the reactive section and stages in the nonreactive zones. The residence time and hold-up on the stages of the nonreactive zones are roughly the same for both configurations, but the liquid hold-up and the residence time in a staged reactive section are about 10 times larger than in a packed column configuration. Any disturbance in the feed will propagate in the packed reactive section much quicker than it does in a staged reactive section. Intuitively, one would conclude that the packed column is in general more sensitive to disturbances than a trayed column. This only holds when operating at a high-conversion steady state where the iso-butene concentrations in the rectifying section are roughly the same for both configurations. In this case the dynamics are predominantly influenced by the difference in residence times. The system migrates from a high- to a low-conversion steady

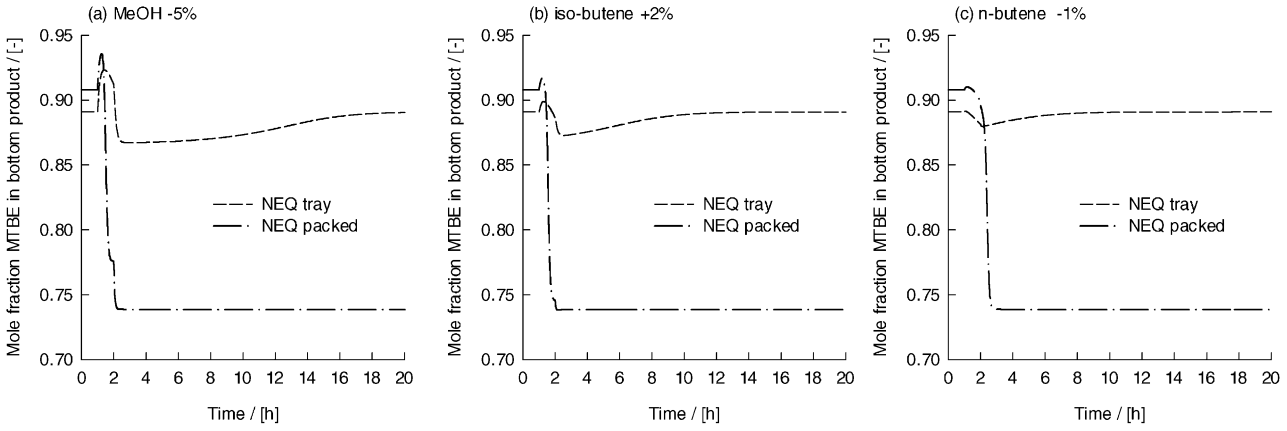

Fig. 15. Dynamic response to (a) − 5% MeOH, (b) + 2% iso-butene and (c) − 1% n-butene feed flow perturbations, 1 h after column start-up and lasting for 1 h. Starting steady state is the high-conversion one. Comparison of NEQ models for tray and packed column configurations.

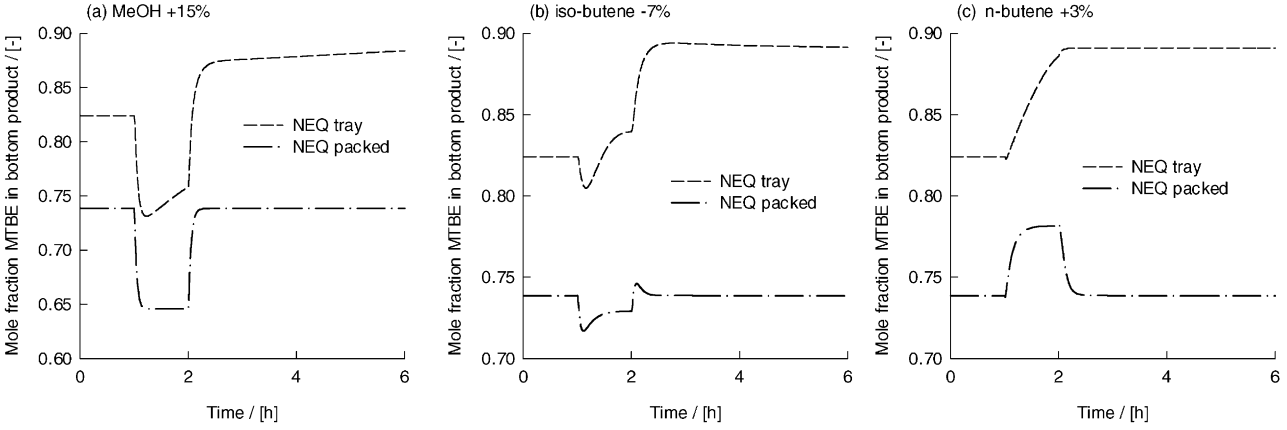

Fig. 16. Dynamic response to (a) + 15% MeOH, (b) − 7% iso-butene and (c) + 3% n-butene feed flow perturbations, 1 h after column start-up and lasting for 1 h. Starting steady state is the low-conversion one. Comparison of NEQ models for tray and packed column configurations.

state as soon as the iso-butene recycle reaches a point where it triggers high MTBE production rates at the top of the reactive section. The quicker a disturbance propagates, the easier the system suffers a transition. This confirms our observations where the size and duration of a perturbation causing a transition is in general smaller for a packed than for a trayed column configuration.

Operating at a low-conversion steady state we also have to consider the initial iso-butene accumulation in the rectifying section at steady state. The reaction rate at the top of the reactive section is mainly determined by the iso-butene supply from the rectifying section. When shifting from a low- to a high-conversion steady state iso-butene has to be "washed-out" in order to decrease the MTBE production in the reactive section beneath. Keeping in mind that the residence times in the rectifying section are roughly the same for both configurations, a steady-state transition depends on the type, size and duration of the perturbation, on the propagation in the column, as well as on the accumulation of iso-butene in the rectifying section at low-conversion steady state. The packed column configuration exhibits a higher iso-butene concentration in the rectifying section and higher reaction rates regarding the MTBE production and decomposition. The reason for this is a lower mass transfer resistance caused by higher interfacial area in the reactive section. Although, a disturbance propagates much faster in a packed reactive section, the high iso-butene concentration in the rectifying section makes it less sensitive to perturbations.

In order to illustrate this we focus on the top of the reactive distillation column. Fig. 17(a) shows dynamic responses of the iso-butene mole fraction on stage 3 and the MTBE production rates on the stage (or equivalent packing section) below. At the initial (low-conversion) steady state the iso-butene mole fraction in the rectifying section of the packed column is almost twice as high; see $t = 0$ in Fig. 17(a). When the iso-butene feed is decreased by 7% at $t = 1$ h, the disturbance propagates faster in the packed section (indicated by the steep slope of the

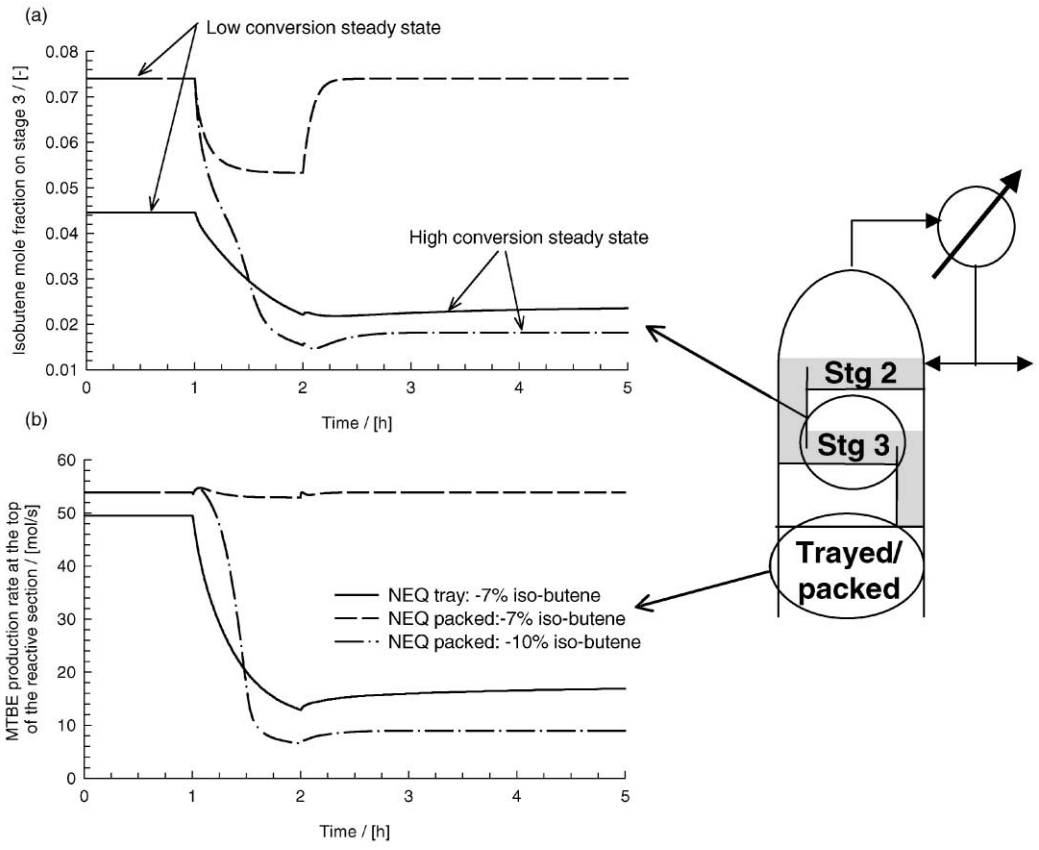

Fig. 17. Dynamic responses at the top of the column to − 7 and − 10% iso-butene feed flow perturbations, 1 h after column start-up and lasting for 1 h. Starting steady state is the low-conversion one. Comparison of NEQ models for tray and packed column configurations.

iso-butene mole fraction on stage 3) than it does in case of a trayed column. This, however, does not significantly affect the production rates in the top part of the packed reactive section. The iso-butene supply from the rectifying section is sufficient to sustain the MTBE production; see Fig. 17(b). The system reverts back to its initial low-conversion steady state; see also Fig. 16(b).

In case of a trayed column configuration the 7% decrease of iso-butene is sufficient enough to decrease the iso-butene concentration in the rectifying section, and so mitigate the MTBE production. Already after approximately 15 min the iso-butene mole fraction is reduced by a quarter and the MTBE production rate has been halved; see Fig. 17(b). The system enjoys a transient to the high-conversion steady state; see also Fig. 16(b).

Decreasing the iso-butene feed further to − 10% causes also the packed column to shift to a high-conversion steady state. Shortly after the perturbation the iso-butene in the rectifying section gets "washed-out". The internal dynamics are quick due to low residence time in the packed section, and so the MTBE production rates at the top of the packed section are restricted rapidly.

The hardware design has a significant impact on the open loop dynamics of reactive distillation column. The residence time distribution in the column and its steady-state behaviour determine the underlying mechanism for possible steady-state transitions. A packed reactive section with faster dynamics need not be more sensitive, as illustrated in the examples above.

5. Simulations of the experiments on TAME synthesis

Mohl et al. (1999) have recently published experimental data on the synthesis of TAME in a packed RD column. The column consists out of two sections, a reactive section at the top of the column and a stripping section in order to purify TAME. The column diameter is 80 mm and each section has a height of 0.5 m. The feed is located in the middle of the column between the reactive and inert packing. Mohl et al. (1999) reported experimental evidence of multiple steady states for a reboiler load of 340 W. The phenomenon of steady-state multiplicity can be reproduced using the NEQ model, wherein the reaction is treated as pseudo-homogeneous and the liquid phase nonideality is described by the Wilson model. The NEQ model is modelled by 20 slice per section using Onda et al. (1968) correlation for calculating the mass transfer coefficients. The liquid hold-up in

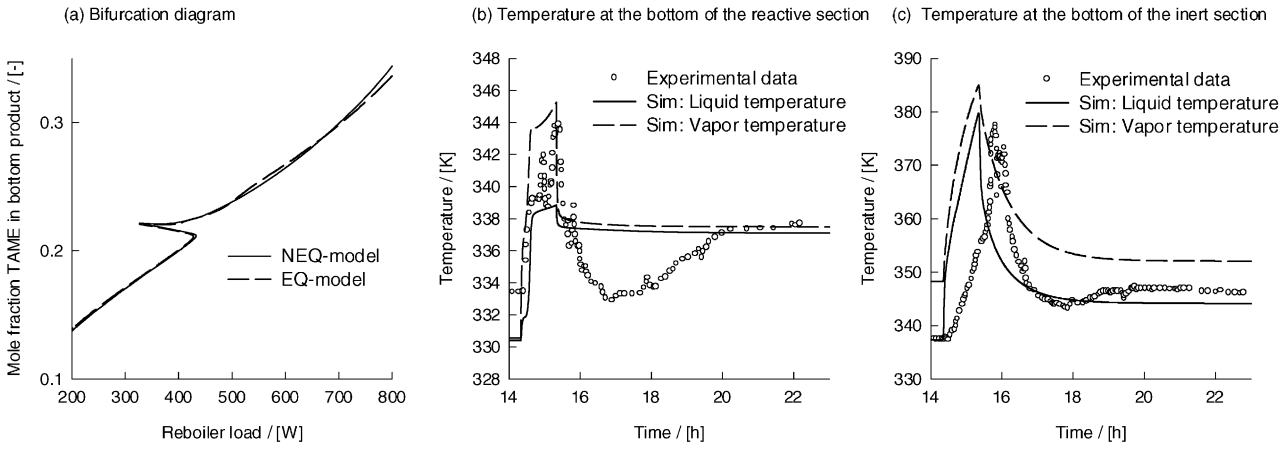

Fig. 18. (a) Bifurcation diagram for synthesis of tertiary amyl-ether (TAME) in packed RD column using EQ and NEQ models. Responses to switching of feed to pure TAME calculated with NEQ model (b) at the bottom of the reactive section and (c) at the bottom of the stripping section. Experimental data are from Mohl et al. (1999).

the packing is computed according to Mackowiak (1991) as described by Kruse, Frieg, Wozny, Heromin, and Johannisbauer (1995). Column design and specification have been taken over from Mohl et al. (1999). No further adjustments were required to obtain a reasonable match of the temperature column profiles, which are in good agreement with simulations reported by Mohl et al. (1999). The details of the steady-state simulation procedure have been published earlier; see Higler et al. (2000). Fig. 18(a) shows the bifurcation diagram for varying heat duty. An EQ model using 5 stage per section with an efficiency of 0.7 and the NEQ model results almost coincide. In contrast to the previously studied MTBE column mass transfer resistances appear to be circumstantial for the column configuration under consideration.

In the experiment, the liquid feed to the column was switched to pure TAME for 1 h. The drums in the reboiler and condenser had been estimated to possess a volume of 1 l. The experiments showed a transition from the low- to the high-conversion steady state. Fig. 18(b) presents the temperature beneath the reactive section and Fig. 18(c) beneath the stripping section, respectively. The simulation of the feed perturbation, using the NEQ model developed in this paper is also shown in Fig. 18(b) and (c). The solid line shows the liquid and the dashed line the vapour temperature. It is noteworthy to mention that parts of the column are predicted not to be in thermal equilibrium, since an almost binary mixture of TAME and n-pentane with large differences in boiling and dew point temperatures gets totally reboiled.

The dynamic behaviour of the laboratory column is strongly influenced by the high liquid hold-up in the porous catalyst (Mohl et al., 1997, 1999). Although, a constant fractional liquid hold-up in the packing has been accounted for, the pseudo-homogeneous model is obviously not able to describe intraparticle mass transfer, energy and mass storage. The model also does not account for possible influences, such as changes in operating pressure when switching feed or responses of controllers. Since these phenomena are not modelled, the simulations predict a rapid temperature and composition change at the beginning and end of the perturbation. Despite the limitations of the model, the essential features of the steady-state transitions are reproduced lending credence to the dynamic model developed in this paper.

6. Concluding remarks

We have developed a rigorous dynamic NEQ stage model for RD columns. The rich dynamic features of RD columns have been illustrated by a case study for MTBE synthesis. Depending on the type, size and duration a feed flow perturbation can cause a transition from one steady state to another. The underlying mechanism triggering these transitions was revealed by means of studying the internal iso-butene recycle flows.

The EQ and NEQ models show some quantitatively different responses to feed flow disturbances of MeOH, iso-butene and n-butene. The effect of mass transfer on internal iso-butene recycle predominantly causes this. An EQ model with an efficiency of 0.8 is generally less prone to steady-state transitions.

The dynamics of the open loop column are strongly influenced by the column specification. A constant reboiler heat duty or constant bottom molar flow rate specification results in an intrinsic different dynamic behaviour.

The dynamic response of an RD column is also sensitive to the hardware choice. The open loop dynamics are predominately influenced by the storage capacities (at steady state) and residence times in particular when

focussing on hybrid columns. It is clear that the control strategies to be adopted will also be determined by the precise configuration of the reactive section.

Notation

a interfacial area per unit volume, m^{-1}
A interfacial area, m^2
A_{bub} active (bubbling) area on tray, m^2
c number of components in the mixture, dimensionless
c_t total concentration, mol/m^3
$Đ_{i,k}$ Maxwell–Stefan diffusivity, m^2/s
E energy hold-up, J
$\mathbb{E}$ energy transfer rate, J/s
F feed stream, mol/s
h_{cl} clear liquid height, m
h_t tray spacing, m
h_w weir height, m
H molar enthalpy, J/mol
h heat transfer coefficient, W/m^2 K
K vapour–liquid equilibrium constant, dimensionless
L liquid flow rate, mol/s
L_M interchange liquid flow rate between horizontal rows of cells, mol/s
$M_{i,j}$ molar hold-up of component i on stage j, mol
$\mathbb{N}$ mass transfer rate, mol/s
p_j stage pressure, Pa
Q heat duty, J/s
r number of reactions, dimensionless
$R_{i,j}$ reaction rate, mol/m^3 s
$\mathbb{R}$ gas constant, J/mol K
T temperature, K
V vapour flow rate, mol/s
W weir length, m
x mole fraction in the liquid phase, dimensionless
y mole fraction in the vapour phase, dimensionless
z mole fraction in the feed stream, dimensionless

Greek letters

ε volumetric hold-up of phase, m^3
δ diffusion film thickness, m
η dimensionless coordinate, dimensionless
κ mass transfer coefficient, m/s
μ chemical potential, J/mol

Subscripts

i component index
j stage index
k index
I referring to interface
t total

Superscripts

F referring to feed stream
L referring to liquid phase
Lf referring to liquid diffusion film
V referring to vapour phase
Vf referring to vapour diffusion film

Acknowledgements

Partial support for our work comes from BP-Amoco Chemicals. RK and RB acknowledge financial support from the Netherlands Organisation for Scientific Research (NWO) in the form of a "programmasubsidie" for development of novel concepts in reactive separations technology.

References

Abufares, A. A., & Douglas, P. L. (1995). Mathematical modeling and simulation of an MTBE catalytic distillation process using SPEEDUP and AspenPlus. *Chemical Engineering Research and Design, Transactions of the Institution of Chemical Engineers Part A*, *73*, 3–12.

Alejski, K., & Duprat, F. (1996). Dynamic simulation of the multicomponent reactive distillation. *Chemical Engineering Science*, *51*, 4237–4252.

Barker, P. E., & Self, M. F. (1962). The evaluation of liquid mixing effects on a sieve plate using unsteady and steady state tracer techniques. *Chemical Engineering Science*, *17*, 541–554.

Bartlett, D. A., & Wahnschafft, O. M. (1998). Dynamic simulation and control strategy evaluation for MTBE reactive distillation. In J. F. Pekny, & G. E. Blau (Eds.), *Foundations of computer-aided process operation*. American Institute of Chemical Engineers Symposium Series, vol. 320 (pp. 315–321). New York: A.I.Ch.E.

Baur, R., Higler, A. P., Taylor, R., & Krishna, R. (2000). Comparison of equilibrium stage and nonequilibrium stage models for reactive distillation. *Chemical Engineering Journal*, *76*, 33–47.

Bennett, D. L., Agrawal, R., & Cook, P. J. (1983). New pressure drop correlation for sieve tray distillation columns. *American Institute of Chemical Engineers Journal*, *29*, 434–442.

Bravo, J. L., Pyhalathi, A., & Jaervelin, H. (1993). Investigations in a catalytic distillation pilot plant: Vapour/liquid equilibrium, kinetics and mass transfer issues. *Industrial and Engineering Chemistry Research*, *32*, 2220–2225.

Bulirsch, R., & Stoer, J. (1966). Numerical treatment of ordinary differential equations by extrapolation methods. *Numerical Mathematics*, *8*, 1–13.

Danner, R. P., & Daubert, T. E. (1983). *Manual for predicting chemical process design data.*. New York: American Institute of Chemical Engineers.

Doherty, M. F., & Buzad, G. (1992). Reactive distillation by design. *Chemical Engineering Research and Design, Transactions of the Institution of Chemical Engineers Part A*, *70*, 448–458.

Espinosa, J., Martinez, E., & Perez, G. A. (1994). Dynamic behavior of reactive distillation columns, Equilibrium systems. *Chemical Engineering Communications*, *128*, 19–42.

Fair, J. R., Steinmeyer, D. E., Penney, W. R., & Croker, B. B. (1997). Gas absorption and gas–liquid system design. In D. W. Green, & J. O. Maloney (Eds.), *Perry's chemical engineers' handbook* (7th Ed.), New York: McGraw-Hill (Section 14).

Grosser, J. H., Doherty, M. F., & Malone, M. F. (1987). Modeling of reactive distillation systems. *Industrial and Engineering Chemistry Research*, *26*, 983–989.

Güttinger, T. E., & Morari, M. (1999a). Predicting multiple steady states in equilibrium reactive distillation. 1. Analysis of nonhybrid systems. *Industrial and Engineering Chemistry Research*, *38*, 1633–1648.

Güttinger, T. E., & Morari, M. (1999b). Predicting multiple steady states in equilibrium reactive distillation. 2. Analysis of hybrid systems. *Industrial and Engineering Chemistry Research*, *38*, 1649–1665.

Hauan, S., Hertzberg, T., & Lien, K. M. (1995). Why methyl tert butyl ether production by reactive distillation may yield multiple solutions. *Industrial and Engineering Chemistry Research*, *34*, 987–991.

Higler, A., Krishna, R., & Taylor, R. (1999a). A nonequilibrium cell model for multicomponent (reactive) separation processes. *American Institute of Chemical Engineers Journal*, *45*, 2357–2370.

Higler, A., Krishna, R., & Taylor, R. (1999b). A non-equilibrium cell model for packed distillation columns. The influence of maldistribution. *Industrial and Engineering Chemistry Research*, *38*, 3988–3999.

Higler, A., Krishna, R., & Taylor, R. (2000). Non-equilibrium modelling of reactive distillation: A dusty fluid model for heterogeneously catalysed processes. *Industrial and Engineering Chemistry Research*, *39*, 1596–1607.

Higler, A. P., Taylor, R., & Krishna, R. (1998). Modeling of a reactive separation process using a nonequilibrium stage model. *Computers & Chemical Engineering*, *22*, S111–S118.

Higler, A. P., Taylor, R., & Krishna, R. (1999c). Nonequilibrium modelling of reactive distillation: Multiple steady states in MTBE synthesis. *Chemical Engineering Science*, *54*, 1389–1395.

Higler, A. P., Taylor, R., & Krishna, R. (1999d). The influence of mass transfer and liquid mixing on the performance of reactive distillation tray column. *Chemical Engineering Science*, *54*, 2873–2881.

Hofhuis, P. A. M., & Zuiderweg, F. J. (1979). Sieve plates: dispersion density and flow regimes. *Institution of Chemical Engineers Symposium Series*, *Series No. 56* (pp. 2.2/1–2.2/26).

Jacobs, R., & Krishna, R. (1993). Multiple Solutions in reactive distillation for methyl-tert-butyl ether synthesis. *Industrial and Engineering Chemistry Research*, *32*, 1706–1709.

Jones Jr., E. M. (1985). Contact structure for use in catalytic distillation. US Patent 4536373.

Kooijman, H. A. (1995). *Dynamic nonequilibrium column simulation*. Ph.D. dissertation, Clarkson University, Potsdam, USA.

Kooijman, H. A., & Taylor, R. (1995). A dynamic nonequilibrium model of tray distillation columns. *American Institute of Chemical Engineers Journal*, *41*, 1852–1863.

Kreul, L. U., Gorak, A., Dittrich, C., & Barton, P. I. (1998). Dynamic catalytic distillation: Advanced simulation and experimental validation. *Computers & Chemical Engineering*, *22*, S371–S378.

Krishna, R., & Wesselingh, J. A. (1997). The Maxwell–Stefan approach to mass transfer. *Chemical Engineering Science*, *52*, 861–911.

Kruse, C., Frieg, G., Wozny, G., Jeromin, L., & Johannisbauer, W. (1995). Experimental verification of the equilibrium stage model for the dynamics of the multicomponent distillation considering the effects of energy loss. *Industrial and Engineering Chemistry Research*, *34*, 1810–1822.

Kubicek, M. (1976). Algorithm 502, dependence of a solution of nonlinear systems on a parameter. *ACM Transactions on Mathematical Software*, *2*, 98–107.

Kumar, A., & Daoutidis, P. (1999). Modeling, analysis and control of ethylene glycol reactive distillation column. *American Institute of Chemical Engineers Journal*, *45*, 51–68.

Lockett, M. J. (1986). *Distillation tray fundamentals*. Cambridge, UK: Cambridge University Press.

Mackowiak, J. (1991). *Fluiddynamik von Kolonnen mit modernen Füllkörpern und Packungen für Gas/Flüssigkeitssysteme*. Sauerländer, Aarau.

Michelsen, M. (1976). An efficient general purpose method of integration of stiff ordinary differential equations. *American Institute of Chemical Engineers Journal*, *22*, 594–597.

Moe, H. I., Hauan, S., Lien, K. M., & Hertzberg, T. (1995). Dynamic model of a system with phase and reaction equilibrium. *Computers & Chemical Engineering*, *19*, S513–S518.

Mohl, K. D., Kienle, A., Gilles, E. D., Rapmund, P., Sundmacher, K., & Hoffmann, U. (1997). Nonlinear dynamics of reactive distillation processes for the production of fuel ethers. *Computers & Chemical Engineering*, *21*, S989–S994.

Mohl, K. D., Kienle, A., Gilles, E. D., Rapmund, P., Sundmacher, K., & Hoffmann, U. (1999). Steady state multiplicities in reactive distillation columns for the production of fuel ethers MTBE and TAME: Theoretical analysis and experimental verification. *Chemical Engineering Science*, *54*, 1029–1043.

Onda, K., Takeuchi, H., & Okumoto, Y. (1968). Mass transfer coefficients between gas and liquid phases in packed columns. *Journal of Chemical Engineering Japan*, *1*, 56–62.

Perez-Cisneros, E., Schenk, M., Gani, R., & Pilavachi, P. A. (1996). Aspects of simulation, design and analysis of reactive distillation operations. *Computers & Chemical Engineering*, *20*, S267–S272.

Rehfinger, A., & Hoffmann, U. (1990a). Kinetics of methyl-tert-butyl ether liquid phase synthesis catalyzed by ion exchange resin. I — Intrinsic rate expression in liquid phase activities. *Chemical Engineering Science*, *45*, 1605–1616.

Rehfinger, A., & Hoffmann, U. (1990b). Kinetics of methyl-tert-butyl ether liquid phase synthesis catalyzed by ion exchange resin. II — Macropore diffusion of MeOH as rate controlling step. *Chemical Engineering Science*, *45*, 1619–1626.

Reid, R. C., Prausnitz, J. M., & Poling, B. M. (1988). *The properties of gases and liquids* (4th ed.). New York: McGraw-Hill.

Ruiz, C. A., Basualdo, M. S., & Scenna, N. J. (1995). Reactive distillation dynamic simulation. *Chemical Engineering Research and Design, Transactions of the Institution of Chemical Engineers Part A*, *73*, 363–378.

Scenna, N. J., Ruiz, C. A., & Benz, S. J. (1998). Dynamic simulation of startup procedures of reactive distillation columns. *Computers & Chemical Engineering*, *22*, S719–S722.

Schrans, S., de Wolf, S., & Baur, R. (1996). Dynamic simulation of reactive distillation, an MTBE case study. *Computers & Chemical Engineering*, *20(Suppl)*, S1619–S1624.

Seader, J. D., & Henley, E. J. (1998). *Separation process principles*. New York: Wiley.

Sneesby, M. G., Tadé, M. O., & Smith, T. N. (1998a). Mechanistic interpretation of multiplicity in hybrif reactive distillation: Physically realisable cases. *Industrial and Engineering Chemistry Research*, *37*, 4424–4433.

Sneesby, M. G., Tadé, M. O., & Smith, T. N. (1998b). Steady state transitions in the reactive distillation of MTBE. *Computers & Chemical Engineering*, *22*, 879–892.

Stichlmair, J. G., & Fair, J. R. (1998). *Distillation principles and practice*. New York: Wiley-VCH.

Sundmacher, K., & Hoffmann, U. (1994). Multicomponent mass transfer and energy transport on different length scales in a packed reactive distillation column for heterogeneously catalyzed fuel ether production. *Chemical Engineering Science*, *49*, 4443–4464.

Taylor, R., Kooijman, H. A., & Hung, J. S. (1994). A second generation nonequilibrium model for computer simulation of multicomponent separation processes. *Computers & Chemical Engineering*, *18*, 205–217.

Taylor, R., & Krishna, R. (2000). Modelling reactive distillation. *Chemical Engineering Science*, *55*, 5183–5229.

Taylor, R., & Krishna, R. (1993). *Multicomponent mass transfer*. New York: Wiley.

Wayburn, T. L., & Seader, J. D. (1987). Homotopy continuation methods for computer aided process design. *Computers & Chemical Engineering*, *11*, 7–25.

Wesselingh, J. A., & Krishna, R. (2000). *Mass transfer in multicomponent mixtures*. Delft: Delft University Press.